

This is an Open Access document downloaded from ORCA, Cardiff University's institutional repository: <https://orca.cardiff.ac.uk/id/eprint/141461/>

This is the author's version of a work that was submitted to / accepted for publication.

Citation for final published version:

Davies, Robert , Jefferson, Anthony and Gardner, Diane 2021. Development and testing of vascular networks for self-healing cementitious materials. *Journal of Materials in Civil Engineering* 33 (7) 10.1061/(ASCE)MT.1943-5533.0003802

Publishers page: [https://ascelibrary.org/doi/10.1061/\(ASCE\)MT.1943-...](https://ascelibrary.org/doi/10.1061/(ASCE)MT.1943-...)

Please note:

Changes made as a result of publishing processes such as copy-editing, formatting and page numbers may not be reflected in this version. For the definitive version of this publication, please refer to the published source. You are advised to consult the publisher's version if you wish to cite this paper.

This version is being made available in accordance with publisher policies. See <http://orca.cf.ac.uk/policies.html> for usage policies. Copyright and moral rights for publications made available in ORCA are retained by the copyright holders.



Development and Testing of Vascular Networks for Self-healing Cementitious Materials

Robert Davies, Ph.D., CEng¹, Tony Jefferson, Ph.D., CEng², and Diane Gardner, Ph.D., CEng³

¹Lecturer, Cardiff University, School of Engineering, Queens Buildings, The Parade, Cardiff, United Kingdom, CF24 3AA. (Corresponding Author) Email: DaviesRE11@Cardiff.ac.uk

²Professor, Cardiff University, School of Engineering, Queens Buildings, The Parade, Cardiff, United Kingdom, CF24 3AA. Email: JeffersonAD@Cardiff.ac.uk

³Senior Lecturer, Cardiff University, School of Engineering, Queens Buildings, The Parade, Cardiff, United Kingdom, CF24 3AA. Email: GardnerDR@Cardiff.ac.uk

ABSTRACT

The success of self-healing cementitious materials relies on their ability to repeatedly heal over the lifetime of the material. Vascular networks have a distinct advantage over other self-healing techniques whereby the healing agent in the network can be routinely replenished. The aim of this study was to develop a multi-use vascular network that can be re-used over the lifetime of a structure, to enable repeated self-healing events in cementitious materials. The feasibility and self-healing efficacy of novel 2D vascular networks in concrete beams were tested on laboratory-scale specimens before being trialled in-situ on larger, structural-scale elements. The vascular networks were formed via linear interconnecting hollow channels filled with a healing agent which is delivered to zones of damage under an externally supplied pressure. This technique was reproducible at large scale and channels were re-filled over a test period of 6 months. Of the two healing agents used in this study, sodium silicate (SS) proved easier to handle and supply into the vascular network, but cyanoacrylate (CA) offered greater strength recovery (up to 90%) in a relatively short timescale. The presence of flow networks in the cover concrete tended to act as a crack initiator and this was particularly

24 evident in the larger scale specimens. Nevertheless, the potential to enhance and enable multi-scale
25 healing in cementitious materials has been demonstrated.

26 **INTRODUCTION**

27 Our society is very much dependent on the security and durability of our civil engineering
28 infrastructure, much of which is constructed from concrete. Indeed, concrete remains one of the
29 most widely used construction materials in the world today. However, concrete degradation and
30 concrete cracking is still considered a major problem (Gardner et al. 2018), the causes of which
31 result from thermal effects, early age shrinkage, mechanical loading, deleterious chemical reactions
32 or a combination of these actions on structures (Concrete Society 2010). These issues affect the
33 durability of concrete structures and lead to a service life far shorter than that desired. The concept
34 of a material with a self-repairing or self-healing capability has been identified as a potential
35 solution to this problem. A state-of-the-art paper produced by the Self-healing as prevention repair
36 of concrete structures (SARCOS) COST Action group describes the breadth of this novel research
37 area and explores the latest innovations in the field of self-healing cementitious materials (De Belie
38 et al. 2018).

39 The techniques used in self-healing concrete can be broadly classified into three groups (De Be-
40 lie et al. 2018; Van Tittelboom and De Belie 2013); Autogenous and non-encapsulated autonomous
41 self-healing (which include autogenous healing, stimulated autogenous healing with the use of min-
42 eral additions, crystalline admixtures, superabsorbent polymers and non-SAP polymer additions),
43 self-healing bio-concrete, and encapsulated autonomous self-healing. Encapsulation techniques
44 include the use of polymer and mineral-based healing agents, which are delivered into the cracked
45 areas in concrete through micro-encapsulation (diameter capsules < 1 mm), macro-encapsulation
46 or vascular network technologies embedded in the concrete (Sidiq et al. 2019; Xue et al. 2019).

47 The vascular network technique adopts a biomimetic approach to healing cracks by delivering
48 healing agents to the damage location, in a similar manner to the human cardiovascular or plant
49 vascular tissue systems. The vascular network has several advantages over closed systems, such as
50 being able to supply different healing agents, over various time scales and at different rates to the

51 damage location (Blaiszik et al. 2010) in order to treat a variety of damage scenarios.

52 The first use of capillary networks in cementitious materials was reported by Dry (1994).
53 Originally, these networks comprised discrete capillary capsules embedded within the cementitious
54 matrix (Van Tittelboom et al. 2011; Van Tittelboom and De Belie 2013), which were subsequently
55 replaced by continuous glass capillaries extending throughout the specimen with external supply
56 reservoirs (Mihashi et al. 2001; Joseph et al. 2010). Glass capillaries have been embedded into
57 frame structures (Dry and McMillan 1996) and also cast into bridge decks for full-scale trials (Dry
58 1999; Dry 2001). However, due to the challenges associated with the use of these systems for
59 in-situ concrete structures, in particular the increased time required to place the capillary tubes
60 prior to casting (Van Tittelboom et al. 2016) and the fragility of the capillary tubes during casting,
61 these systems have been predominantly limited to laboratory testing and evaluation. Moreover,
62 Van Tittelboom et al. (2016) note that the positive self-healing efficiencies achieved through the
63 careful placement of the capillary tubes within a mould at small-scale, may be diminished at large-
64 scale, if methods employed for the ready inclusion of capillary tubes in a mix results in their random
65 orientation within the section.

66 To overcome some of these challenges the glass capillaries have been replaced with channels
67 formed through a variety of other methods: One early approach was the embedment of ethylene
68 vinyl acetate polymer pipes containing conductive helical wire and healing agent in the cementitious
69 matrix (Nishiwaki et al. 2010). Selective heating at the location of a crack released healing agent
70 directly into the damage location. The second approach was the formation of hollow channels
71 via the removal of smooth small diameter steel rods after 24 hours of concrete curing (Dry 1999;
72 Pareek and Oohira 2011) and the third was the use of porous concrete cylinders surrounded by a
73 standard concrete mix (Sangadji and Schlangen 2012). Nevertheless, the formation of these novel
74 flow networks is not without difficulty since they rely on the timely and successful removal of
75 channel forming elements in the former and require a two-stage construction process in the latter.
76 Moreover, these techniques are currently limited to a two-dimensional format. Varying degrees of
77 success have been reported on the performance of flow networks, such as an enhanced load carrying

78 capacity from beams healed with a 2-part epoxy (Dry et al. 2003) and greater post peak ductility
79 for beams healed with cyanoacrylate (Joseph et al. 2010).

80 Critical to the success of a vascular network is the correct selection of healing agent. The
81 capillary flow of the healing agent is highly dependent on its flow properties, namely its viscosity,
82 wettability and surface tension in a cementitious environment, whilst its healing ability will depend
83 on its compatibility and reaction with the host matrix. The success or otherwise of a range of healing
84 agents including sodium silicate (Formia et al. 2015; Kanellopoulos et al. 2015); polyurethane
85 ((Gilabert et al. 2017; Belleghem et al. 2018); cyanoacrylates (Gardner et al. 2012; Gardner et al.
86 2014; Huang et al. 2014); and epoxies (Perez et al. 2015; Li et al. 2017) has been widely reported.
87 The introduction of pressurised vascular networks, as trialled in self-healing polymer materials by
88 Hamilton et al. (2011), greatly assists the extent of flow and infiltration of the healing agent into
89 micro-cracked zones of damage and is worthy of further investigation in cementitious materials.

90 This paper describes a novel method for the formation of a two-dimensional vascular network for
91 cementitious materials, including its deployment in slabs and structural scale elements. The design
92 of the network facilitates repeated healing events over the lifetime of a cementitious structure. In
93 addition, the first full account of the use of vascular networks in a site trial is reported herein. The
94 paper is structured as follows:

- 95 • Section 2 provides an overview of a series of preliminary investigations concerning the man-
96 ufacture of the vascular network, specifically the influence of channel diameter, joint/node
97 design and network pressure.
- 98 • Section 3 presents the experimental details concerning the application of vascular networks
99 in a range of structural elements, namely small beams, large beams, a slab and a wall panel.
100 It also presents the selection and justification of the healing agent used in the study.
- 101 • Section 4 presents the experimental results and reports the healing efficiencies of structural
102 elements with various network configurations.

103 **PRELIMINARY INVESTIGATIONS**

Channel and Connection Design

A series of preliminary investigations was conducted to establish a successful and repeatable method of forming vascular networks in cementitious materials. The criteria for their formation was: (i) to cause no damage to the cementitious matrix; (ii) to be capable of practical application to both laboratory and in-situ structural sized specimens and (iii) to allow the flow of liquid throughout the entire network in one and two dimensions. The most practical approach is to form a network during the concrete casting process, since this eliminates the potential for damage to the concrete in its hardened state. The novel method proposed in this paper employs the embedment of plastic tubing, which is extracted from hardened concrete to leave permanent one-dimensional and two-dimensional interconnecting channels. Both polyolefin (TE Connectivity CGPT clear heat shrink tubing) and polyurethane (SMC TU series) tubing proved successful candidates for this. In both instances, the tubes were placed through holes in the concrete specimen mould walls and held in place with small clamps on the outside of the moulds, as shown in Fig. 1a.

The polyolefin tubing had an outer diameter of 3.2 mm and a shrinkage ratio of 2:1 at 80 °C. This tubing was flexible and compressible and to prevent compression during placement of concrete the network required pressurisation with water. After casting, curing and de-moulding of the prism specimen, the polyolefin tubes were flushed with water at a temperature of 85 °C, which triggered tube shrinkage and thereby allowed them to be easily removed from the specimen.

The polyurethane tubing had an outer diameter of 4 mm and was selected for its smooth outer surface properties, relatively high stiffness and high tensile strength. The polyurethane tubes were robust enough to withstand the casting process without the need for pressurisation. After casting, curing and de-moulding, the polyurethane tubes were pulled out of the specimen. The radial contraction of the tube, when under tension, breaks the bond between the tube surface and the concrete, thus permitting the tubes to be removed with relative ease.

Neither tubing material required the application of a special coating. Preliminary experiments showed that the tubing placed as loops in small prismatic concrete beams could also be easily removed, therefore only requiring one accessible surface during casting. This would be advantageous

131 for casting concrete foundations or other structural elements with limited accessible surfaces after
132 casting. In subsequent studies with larger specimens, special coatings were applied to the tubes
133 guarantee their removal.

134 A plan 2-D network was created by taking advantage of the voids left by removal of the tubes
135 and by the contact points between overlapping tubes, as illustrated by the schematic in Fig. 1b.
136 The area of the contact points is maximised by using a weaving tube pattern shown in Fig. 1c.
137 The voids left by the contact points are shown to be sufficiently large to allow the healing agent to
138 flow. However, they depend on the tubes being tightly tensioned against each other and increase the
139 complexity associated with the placement of the tubes in the mould. To overcome these challenges,
140 a bespoke connection was designed and manufactured from Polylactic Acid (PLA) using a 3D
141 printer (Ultimaker 2, Fused filament fabrication). This connection created a dedicated flow channel
142 between the perpendicular voids, as shown in Fig. 1d, and had the added advantage of securing the
143 tubing in position during the casting stage as evidenced in Fig. 1e. Fig. 1f shows the bespoke 2D
144 PLA connection used for the larger panels, in which the angles between the tubes are set at 26.6° .
145 The void shown is used to tie the connection to the reinforcement and when the tubing is removed
146 from the concrete after casting, the PLA connections remain in situ.

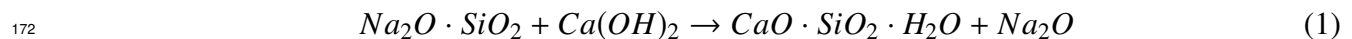
147 **Healing Agent Selection**

148 It is widely regarded that the choice of healing agent is primarily governed by the self-healing
149 application, with particular importance placed on the temporal and spatial nature of the dam-
150 age/healing event (Maes et al. 2014; Van Tittelboom and De Belie 2013; Mostavi Ehsan et al.
151 2015). In this study, cyanoacrylate (CA) and sodium silicate (SS) were selected for use in the
152 vascular networks.

153 CA has been used in many self-healing applications (Li et al. 1998; Dry 2000; Joseph et al. 2010),
154 and is employed here due to its low viscosity, rapid curing time and strong potential to achieve
155 repeated healing events within a short timescale. The ethyl-2-cyanoacrylate resin polymerises
156 rapidly in small crack widths (<0.5 mm) in the presence of hydroxide ions, which are available
157 from moisture within the crack plane, or calcium hydroxide present in the cement matrix. CA

158 has been shown to offer advanced healing from its ability to infiltrate not only the macro-cracks
159 but also the micro-cracked area of the fracture process zone (Joseph et al. 2010). Nevertheless,
160 the use of CA also attracts a significant number of challenges namely: difficulty in handling due
161 to its rapid bonding ability and high toxicity, its relatively short shelf-life (approx. 6 months)
162 and uncertainty regarding its long-term compatibility with the cementitious matrix. Some of the
163 difficulties encountered with the use of CA in these experiments are described in Section 4.

164 Sodium silicate was chosen for its ability to react chemically with the cementitious matrix and
165 its documented success as an encapsulated healing agent in previous studies (Huang and Ye 2011;
166 Pelletier et al. 2011; Gilford III et al. 2013; Kanellopoulos et al. 2015). Its slower reaction rate
167 and higher viscosity makes it more suitable for site application than the rapidly curing CA. In
168 the presence of water, SS reacts with excess calcium hydroxide, a by-product of clinker hydration,
169 available in the cement matrix to form additional calcium-silicate-hydrate (CSH) gel. The chemical
170 reaction is shown in Eq. 1. It is this additional CSH gel which forms and fills in the crack and leads
171 to the recovery in mechanical and durability-based material properties.



173 **Parametric study on capillary rise and surface coverage of healing agent**

174 Healing agents may be delivered by capillary flow alone, but it has been found that the supply
175 of agents may be improved by pressurising the healing agent fluid (Hamilton et al. 2011). Even a
176 small additional pressure of 0.01 bar allows the healing agent to flow more effectively along the
177 supply channels and into the macro-cracks using the capillary rise mechanism (Gardner et al. 2012;
178 Gardner et al. 2014). The degree of saturation of the crack faces has also been reported to influence
179 the rate and degree of capillary rise of a healing agent (Gardner et al. 2012), whilst the crack width
180 is one of the primary governing factors affecting the final healing agent capillary rise height.

181 In order to examine the above parameters, a series of tests were performed on 75 mm x 75
182 mm x 255 mm concrete beams cast with two 4 mm flow channels, formed using the polyurethane
183 tubing detailed in Section 2. The details of the test series are summarised in Table 1. All of the

184 beams were cured in water (apart from beams in series 3). The beams were tested in a 3-point
185 bending arrangement, as shown in Fig. 2, using a controlled crack mouth opening displacement
186 (CMOD) rate of 0.0001 m/s. The healing agent employed was a SS solution of molar ratio 1:1.5
187 (water : sodium silicate). The SS solution was supplied from an open reservoir on one side, the
188 height of which was adjustable, whilst the other side was left open to atmospheric pressure. Once
189 the CMOD had reached the desired value, SS was released into each of the network channels from
190 the required pressure head. The beams were then unloaded and left in-situ for between 60 and 300
191 seconds, after which time the healing agent was flushed out of the channels using pressurised air
192 and the beams broken in half with a hammer. The extent of the spread of the SS on the crack face
193 was then recorded.

194 The effect of a change in healing agent exposure time (as per series 2) can be seen in Fig. 3.
195 The black marker outline shows the extent of the healing agent spread on the crack face, which is
196 termed the crack coverage. This healing agent crack coverage is expressed as a percentage of the
197 crack plane cross-section.

198 Fig. 4 shows the effect of the various parameters on the healing agent crack coverage. In
199 particular, Fig. 4a shows how increasing the pressure of the healing agent increases its coverage
200 on the crack face (Series 1). Fig. 4b and Fig. 4c consider the effect of the curing regime and age
201 of the specimen on crack coverage respectively. The drier beams (i.e. those cured under ambient
202 room conditions) have lower crack coverages, which may result from a concrete matrix with higher
203 porosity and hence greater absorption of the healing agent into the crack faces, effectively reducing
204 the capillary driving force. The older specimens also show a lower healing agent coverage than the
205 younger specimen. The authors have previously demonstrated that the capillary rise response in
206 older specimens is slower than that in younger specimens (Gardner et al. 2012), and this is thought
207 to be related to the effect of the time dependent development of the mortar microstructure on the
208 dynamic resistive forces acting during capillary flow. The results from the present study suggest
209 that the crack coverage associated with older specimens has yet to reach its optimum level given
210 the chosen exposure times. As shown in Fig. 4d, the crack coverage reduces as the cover to the

211 flow channels increases. This reduction may be due to a smaller crack area above the flow channel,
212 since the residual crack opening at the height of the network is smaller.

213 This short parametric study has shown that there are a number of factors that can affect the
214 initial delivery of the healing agent to the crack surface. A relatively small pressure of 0.001
215 N/mm² can provide 80% coverage at a 0.2 mm crack width. The cover to the flow network ranges
216 between 20 mm and 44 mm from the underside of the beam, which is consistent with placing the
217 flow networks in a typical concrete cover zone. The curing regime and age of specimen do have an
218 impact on the extent of coverage of the healing agent on the crack surface but are not considered
219 critical to the performance of the system.

220 **MAIN EXPERIMENTAL PROGRAMME**

221 **Programme of Study and Experimental Procedure**

222 The main experimental programme of study presented in this paper comprises 6 sets of experi-
223 ments, summarised in Table 2 and the different forms are showing in Fig. 5. Sets 1 to 3 demonstrate
224 the performance of vascular networks in a range of prismatic beam specimens, whilst sets 4, 5
225 and 6 explore the application of the flow network in different structural elements (a 0.6 m x 0.6
226 m slab, a 1 m x 1 m wall panel and 1.8 m x 1 m site trial panel). The purpose of the second
227 group of tests (sets 4 to 6) is to prove the scalability of the technique for industrial applications.
228 The experimental programme also included a set of self-healing site trials on the A465 Heads of
229 the Valleys (HoV), Section 2, highway project near Abergavenny in South Wales. These site trials
230 considered a number of healing systems, including the vascular networks being considered in the
231 present paper. All of the moulds/shutters for the concrete specimens were made from timber. These
232 wooden moulds were prepared by drilling 5 mm diameter holes in the desired position and then
233 threading through the 4 mm (external) diameter polyurethane tubes (see Fig. 1a, 1c, 1e). These
234 tubes were straightened by hand tensioning and fixed in position with small clamps on the outside
235 of the mould. Sets 4 to 6 employed the connectors described in Section 2. The channels typically
236 had 20 mm concrete cover. Release oil (and petroleum jelly for Sets 5 and 6) were applied to the
237 tubes before casting the concrete to guarantee their easy removal from the specimens. A standard

238 concrete mix (see Table 3) was used for all lab specimens, with a slight amendment made to the
239 mix for the site trial. The standard C40/50 concrete was designed to achieve consistency class S3
240 (BS EN 12350-2 2019) with an average compressive strength of 53 MPa.

241 All concrete samples were demoulded after 24 hours and the polyurethane tubes removed im-
242 mediately after demoulding leaving behind hollow channels and the bespoke 3D printed connectors.
243 The chosen concrete curing regime was dependent on the selected self-healing agent. CA poly-
244 merises rapidly with water and as such, the specimens were cured at ambient conditions and dried
245 thoroughly before the healing agent was introduced into the flow network. For SS, the specimens
246 were cured in water at 20 °C and surface dried before testing.

247 **Testing Procedure Sets 1-3**

248 The three-point flexural bending test set-up, shown in Fig. 6, was used for Sets 1 to 3. In
249 these specimens, the healing agent was supplied to the channels using polyurethane supply tubes
250 of external diameter 6 mm and internal diameter 4 mm (See Fig. 6). The supply channel was
251 glued in place using CA. This provided a vascular network of constant diameter from the supply
252 tube throughout the specimen. The healing agent was introduced into the vascular network using
253 a syringe. For Sets 1 to 4 the healing agent was supplied into the vascular network before testing
254 began, whilst in the other sets it was introduced at a later stage. The system was pressurised with
255 air via this supply tube, see Fig. 7a. The pressure in the flow network was controlled and monitored
256 using a regulator and inline digital gauges respectively, as can be seen in Fig. 7b. The pressurised
257 system was closed, in order to maintain a constant pressure in the network before load was applied
258 to the specimen. The pressurised system was also used to flush out the remaining healing agent
259 from the main channels by leaving one outlet open to the atmosphere. This flushing allows repeated
260 healing to take place with a re-supply of healing agent. The loading was controlled via a crack
261 mouth opening displacement (CMOD) feedback loop at a rate of 0.0001 mm/s using an Avery
262 Denison 7152 hydraulic loading machine. For Set 1, the beams were loaded until a CMOD of 0.3
263 mm was recorded, at which point the beams were unloaded and the healing agents (CA and SS)
264 were flushed out of the networks using pressurised air. The beams with CA were reloaded after

265 10 minutes, to allow sufficient time for the CA in the crack plane to cure, whilst the left SS beams
266 were placed in a water tank for 7 days before being reloaded.

267 For Sets 2 and 3, the specimens were loaded until a CMOD of 0.5 mm was recorded. At this
268 point the networks in the Set 2 beams were flushed out and the beams left in-situ for 24 hours to
269 allow further curing of the CA before being retested. Similarly the networks in the Set 3 beams
270 were also flushed out, but the beams were then placed in a water tank for 28 days to promote the
271 reaction of SS, after which time the beams were reloaded.

272 **Testing Procedure Set 4**

273 Fig. 8 shows two configurations of flow networks in a 600 mm square slab mould before casting.
274 In the first configuration (Fig. 8a, specimen 1) the channels were placed at an angle of 45° to the
275 line of the supports (and to the steel reinforcement) whilst in the second configuration (Fig. 8b,
276 specimen 2) the channels were placed perpendicular to the supports. In both cases, the channels
277 were located below the reinforcement and had a cover of 20 mm to the base of the slab. One control
278 slab was also cast which included reinforcement only. Eight 8 mm diameter bars were used in each
279 slab, four in each direction at equal spacing.

280 A loading frame, fabricated from 50 mm square hollow steel sections, provided simple supports
281 on all 4 sides of the slab. The central patch load was applied at a controlled displacement rate of
282 0.005 mm/s through a 100 mm square 25 mm thick steel plate and 8 mm thick fibreboard. The
283 displacement was monitored at the centre on the underside of the slab and at the mid-span of one
284 support. The loading setup can be seen in Fig. 8c. The slab was supplied with healing agent and
285 then loaded to 100 kN, unloaded and cured under moist hessian sacks for 28 days before re-loading
286 for a second time.

287 The set-up used to supply healing agent to the specimens was the same as that employed for
288 sets 1 to 3 (Section 3.2). Initially, all supply channels were clamped at their ends. One by one,
289 each supply channel was opened to the atmosphere and the healing agent introduced via a syringe,
290 ensuring that the whole network was filled in a controlled manner. In lieu of a closed pressure
291 system, the network was filled to give 50 mm of head (0.005 bar) above the network level (Fig. 8c).

Testing Procedure Set 5

The configuration of the flow channels for the 1 m x 1 m x 0.15 m demonstration panel in the laboratory is shown in Fig. 9a. This reinforcement arrangement was chosen to replicate the starter bar reinforcement in the trial wall panels (which are discussed in Section 3). Five 10 mm diameter 500 mm long reinforcement bars at 200 mm spacing were fixed vertically in the bottom of the mould, in addition, an A252 mesh (i.e. 8 mm bars @ 200 mm c/c) was placed adjacent to the front and rear faces of the wall over the entire area. A cover of 30 mm was provided to the outermost reinforcement. The flow network was formed by ten sets of 4 mm diameter polyurethane tubes which were placed within the wall panels at an angle of 26.6° to the horizontal, with a vertical spacing of 100 mm and a cover of 20 mm. Ten injection points, as shown in Fig. 9b, were fitted each side of the panel on the vascular network outlets. The 100 mm long packers, of 10 mm external and 2.7 mm internal diameter, were fitted with a locking tap which allowed each channel to be independently opened and closed as required.

The demonstration panel was loaded in the laboratory to induce cracking in the panel. During loading, the wall panel was supported along on two parallel edges (i.e. the top and bottom edges in Fig. 9a) and a horizontal crack was induced via the application of load through a partial width spreader beam at a distance of 500 mm from the base of the wall panel (Fig. 9c). The panel was loaded to 100 kN, at which point a crack was visible on the surface, although the crack opening was not measured during testing. Once the panel had been loaded and a crack became visible, the panel was unloaded and returned to the upright position. Water was pumped into the flow network through the lowest injection valve at the base of the wall, using a pedal controlled reciprocating pump (DESOI PED-3D). Once the water was seen to flow out of a valve, the valve was closed, forcing the network to fill vertically upwards and expel air through the open valves towards the top of the wall. Once the water reached the topmost valve, the valve was closed. The channels in the flow network had the ability to be emptied and refilled, which supports the potential for repeated damage and healing events.

318 **Testing Procedure Set 6**

319 The full site trial programme (See Davies et al. 2018) examined the performance of a range
320 of self-healing systems and included five separate wall panels. The present paper considers the
321 behaviour of one of these panels that contained a vascular network, which was denoted Panel E.
322 The arrangement of Panel E (1.8 m x 1.0 m x 0.15 m) is shown in Fig. 10a, in which the five pairs
323 of evenly spaced 16 mm starter bars (which projected 500 mm from the base of the wall), A393
324 (10 mm bars @ 200 mm c/c) front and A142 (6 mm bars @200 mm c/c) rear steel reinforcing
325 mesh and timber shutters can be seen. The tubes that formed the flow network were placed in
326 an identical manner to that of Set 5 (i.e. the tubes were at angle of 26.6° to the horizontal and
327 spaced at 100 mm), as illustrated in Fig. 10a. These tubes were placed with a cover of 20 mm. The
328 bespoke 3D-printed PLA connections, shown in Fig. 1f, were used at every intersection of the flow
329 network and tied to the steel reinforcement. After casting, the 4 mm diameter polyurethane tubes
330 were removed by hand with relative ease.

331 The 1800 mm tall panel was loaded 300 mm below its upper edge, which meant the panel acted
332 as a vertical cantilever that as illustrated in Fig. 10c. The load was applied through a 100 mm
333 square 10 mm thick section steel wailing spreader beam using a hollow jack ram system that was
334 anchored to the rear of the reaction wall. When the load reached a certain level (20 kN) a horizontal
335 crack became visible on front surface of the panel, approximately 500 mm above the base of the
336 wall, denoted on figures as crack on section (CoS). As with the laboratory trial panel (Section 3)
337 injection point valves were fitted to each location where the network exited the wall panel. The
338 final as-built wall panel is shown in Fig. 10c, in which the painted speckle pattern for the digital
339 image correlation monitoring system can be seen on the surface of the concrete.

340 **RESULTS AND DISCUSSION**

341 The results of each test set are discussed in this section. The degree of mechanical healing is
342 expressed in terms of two parameters: (i) a strength recovery index (H_P), calculated according to
343 Eq. 2 (Homma et al. 2009; Davies and Jefferson 2017) and (ii) a stiffness recovery index (H_K)
344 shown in Eq. 3, both recovery indexes are illustrated in Fig. 11:

$$H_P = \frac{P_2 - P_0}{P_1 - P_0} \cdot 100 \quad (2)$$

in which P_1 represents the initial peak load (kN); P_0 the load at unloading at a predetermined CMOD (kN); and P_2 the peak load upon reloading (kN). Similarly, for the stiffness recovery index H_K :

$$H_K = \frac{K_2 - K_0}{K_1 - K_0} \cdot 100. \quad (3)$$

K_1 represents the initial stiffness of the beam (N/mm²); K_0 the stiffness during unloading (N/mm²); and K_2 the stiffness upon reloading (N/mm²). The terms in Eq. 2 and 3 are clearly defined when cracking and healing are separated in time, as in Fig. 11, but the indices are less distinct when these processes overlap. In the latter case, it is necessary to use the results of the control specimen to compute the unhealed response values that appear in the indices. However, due to the natural variation of response in these materials the response of the control specimen of a test series may deviate from the response that the healed specimen would have undergone without healing. The indices for such cases are therefore given with a degree of caution and this degree of uncertainty is marked by adding a * superscript to the indices (i.e. H_P^* and H_K^*).

Sets 1 to 3 - Twin 1D Channel Beam Specimens

A typical load versus CMOD response for one CA, one SS and one control beam from Set 1 is given in Fig. 12. The control beam was loaded until a CMOD of 0.3 mm was reached, at which point the beam was unloaded and then immediately reloaded until failure.

The beam containing CA was pressurised to 0.2 bar before the load was applied. The first loading cycle resulted in the formation of a central discrete crack. A drop in pressure in the system was recorded at the time this crack first became visible, which is assumed to coincide with the time at which the CA first entered the crack. This resulted in two primary healing responses, characterised by an increase in the load between a CMOD of 0.1 mm and 0.15 mm and also between 0.25 mm and 0.3 mm. These primary healing responses can be attributed to the short-term curing of the CA.

369 It is interesting to note that two healing peaks occurred in the first loading cycle, which points to
370 multiple damage-healing events. Similar primary healing responses have been observed by Joseph
371 et al. (2010) using comparable healing agents and experimental arrangements. For the CA beams,
372 the unloading response, which is considerably stiffer than that of the control beams, confirms that
373 significant healing has taken place in the first loading cycle. During the second loading cycle an
374 increase in load over and above that recorded upon unloading can be seen.

375 In a similar manner, the SS beams were also pressurised to 0.2 bar and showed evidence of a
376 pressure drop upon crack formation. However, due to the longer chemical reaction time of the SS,
377 there was no indication of primary healing. The beam was unloaded at a CMOD of 0.3 mm and a
378 similar unloading response to the control beam was observed. The peak load upon reloading was
379 higher than the load at unloading and the response showed a recovery in stiffness greater than that
380 of the control beam and comparable to the CA beam.

381 Table 4 shows the strength recovery (HP) and stiffness recovery indices (HK) for set 1 for a
382 typical beam for each healing agent, as presented in Fig. 12. It is clear from Table 4 that CA results
383 in much greater healing in terms of strength recovery (79%) compared to SS (17%). The CA results
384 show more variability with a coefficient of variation (CoV) of 15.5% for the HP compared with
385 3.5% for the SS. This increased variability for CA is almost certainly influenced by the complexity
386 of the damage-healing process in the first loading cycle, which means that there would not have been
387 an even distribution of CA available to cure during the fixed crack healing period. There is clear
388 evidence of two primary healing events in the first loading cycle for cyanoacrylate, a phenomenon
389 observed by other researchers working with similar self-healing systems (Joseph et al. 2010).

390 A typical healing response for Set 2 is presented in Fig. 13. As with set 1, a softening curve
391 is observed following the initial peak load, and at a CMOD of 0.2 mm there is a distinctive rise
392 in load carrying capacity (a primary healing response), which coincided with a drop in network
393 pressure. The average strength recovery (HP*) index for set 2 was 39% with a CoV of 6.7% and
394 the average stiffness recovery index (HK*) was 1.3% with a CoV of 35.9%. In load cycle 2, there
395 is evidence of healing, characterised by a regain in stiffness upon reloading and partial recovery of

396 the initial peak load (P1). The average strength recovery (HP) of the specimens in set 2 was 59.7%
397 with a coefficient of variation of 33.7% and the average stiffness recovery (HK) of 81.6% with a
398 coefficient of variation of 20.9%. The relatively high CoV for the results are linked to the significant
399 difficulties in setting up the experimental arrangement (system pressurisation and premature curing
400 of the CA prior to testing), this level of variability confirms the challenges associated with the use
401 of CA as a healing agent.

402 The results from a typical load versus CMOD response for Set 3 beams is presented in Fig. 14,
403 with particular attention to the unload/reload portion of the response given in Fig. 15. The same
404 trends, as observed in Sets 1 and 2, are also seen in Set 3 with the exception that the drop in pressure
405 at crack formation is less pronounced in this case, which almost certainly is due to the fact that
406 SS has a higher viscosity than the CA. For comparison purposes, Fig. 14 and 15 include a control
407 beam response which was subjected to the same conditions. The average strength recovery (HP)
408 of the set was 5.3% with a coefficient of variation of 34%. The stiffness of the SS beam upon
409 reloading is much greater than the control beam as shown by the stiffness healing index of the SS
410 beam being 4.9% with a coefficient of variation of 60%. The significant difference between the
411 recovery index of SS and CA can be attributed to the crack opening, and the ability of the different
412 healing agents to bridge the crack opening during the healing period. The primary healing action
413 of SS is assumed to be its reaction with surplus calcium hydroxide in the cementitious matrix
414 to form further calcium-silicate-hydrate gel. Natural autogenic healing processes yield the most
415 promising results at crack widths of 0.15 mm or less and at larger crack widths, the potential for
416 autogenic healing diminishes. This suggests that SS would work best in systems that employ other
417 mechanisms to limit crack widths. Moreover, the mechanical healing recovery may be low due to
418 the limited availability of calcium hydroxide in the crack plane, especially since hardened cement
419 paste comprises only 15% calcium hydroxide by volume. Nevertheless, SS remains one of the
420 preferred healing agents due to its long-term compatibility with the host matrix.

Set 4 - 2D Channels in Slab

Fig. 16 shows the load versus CMOD response of the control and vascular network slabs. Cracking became visible when the central displacement reached approximately 1.5 mm, after which cracks continued to develop and propagate until the central displacement reached 6 mm (point 2 on the graph), at which point the slab was unloaded. The crack pattern at point (2) is shown in Fig. 17a and, as may be seen in the photograph, significant leakage of the healing agent from the underside of the slab could be observed at this displacement level. Fig. 17b shows the condition of the underside of the slab after unloading (i.e. at point (3)) and this shows the extent of the healing agent migration from the network to the underside of the slabs radial cracks. During the re-loading phase, the effect of healing on the stiffness is evident, in that the initial gradient of the re-load curve in the healed slab is significantly steeper than the control slab. The stiffness healing index (H_K) for the control slab is 46.3% whereas the SS healed slab is 100.2%. The peak load in the second cycle of the self-healing slab is only 2% above that of the control specimen but the response is noticeably more ductile. This limited increase in peak load is strongly influenced by the presence of reinforcement, which tends to mask the healing response, and affected by the fact that the residual crack openings were relatively large during healing (See Fig. 17b), even though the slab was unloaded during healing period. No additional leakage of healing agent was seen (Fig. 17c) indicating that the initial supply of healing agent was exhausted over the month long healing period. Nevertheless, it is proposed that replenishment of the healing between loading cycles may have allowed further cycles of healing to take place.

The crack pattern for a flow network arrangement aligned with the steel reinforcement, as shown in Fig. 17b, was very similar to the crack pattern exhibited by the control slab. This can be seen in Fig. 17a, b and c. However, in the slab in which the vascular network was aligned at 45° to steel to the steel reinforcement, shown in Fig. 8a, the crack patterns replicated the channel configuration (see Fig. 17d), suggesting that the channels act as crack inducers.

446 **Set 5 - 2D Channels in a Demonstration Panel**

447 Following the testing of the set 4 slabs, and with insight thereby gained of the influence of the
448 network configuration on the resulting crack pattern, a 1 m x 1 m demonstration panel was cast
449 as a preparatory stage to the full site-trial tests. This demonstration panel employed water rather
450 than a healing agent. The results presented in this section are descriptive and qualitative in nature
451 and serve to highlight the changes required in the channel filling techniques and testing procedures
452 in readiness for site-trial applications. Following the loading of the panel and the introduction of
453 the water into the network, a small amount of pressure remained in the system (less than 0.5 bar)
454 and this resulted in water leaking out of the crack, as seen in Fig 18b and 18c. Fig 18d shows
455 the concrete panel after testing and partial drying, where the horizontal and diagonal cracking on
456 the face are visible. The diagonal cracks are concurrent with the flow network, again showing
457 the crack initiation action of the flow channels. There is evidence that the supply mechanism was
458 effective, with the filling technique clearly allowing water to fill the entire vascular network, despite
459 the presence of cracks during the filling stage. The injection valves were capable of not only sealing
460 the network but also retaining a small level of pressure (0.5 bar) within it for time enough to allow
461 sufficient water to pass through the cracks onto the surface of the panel. The network supplied
462 water to the full crack network and this is a positive indication of its ability to deliver healing agents
463 of similar flow characteristics as water, to zones of damage.

464 **Set 6 - Vascular Networks in a Site Trial Wall Panel**

465 The panel was first loaded and unloaded at 36 days after casting. The SS was pumped through
466 the network after a further 111 days which showed that the system was still intact and operable. The
467 healing agent was pumped into the panel using the procedure presented in section 4, as depicted in
468 Fig. 19a, The healing agent flowed out of the cracks, assisted by a pressure of 0.2 bar, as evidenced
469 in Fig. 19b. As soon as the SS became visible on the surface of the panel, the system was drained
470 and each channel flushed with water under gravity. The water flushing technique did not result in
471 additional leakage from the panels front face. Furthermore, it is believed that the flushing process
472 did not remover the SS from the cracks. This is because sodium silicate solution has a high viscosity,

473 when compared to water, and a low water flushing pressure was employed to empty the channels.

474 A digital image correlation (DIC) technique was used to monitor the strains on the front face
475 of the panel. The results, shown in Fig. 19c, give the strain plot for Panel E. The crack pattern
476 observed on Panel E at a load of 20 kN supports previous observations that the network channels
477 act as crack inducers, with the diagonal crack pattern reflecting the form of the vascular network
478 (Fig. 19a and 19b).

479 The panel was reloaded to the original load at 231 days after casting and the load versus
480 displacement results compared pre-and post-healing (see Fig. 20). The presence of substantial steel
481 reinforcement in the panel, masks the influence of healing on the load-displacement response, which
482 made it difficult to quantify the mechanical strength recovery which could be directly attributed
483 to the vascular network. Despite the clear site-trial evidence of healing agent flow into the cracks
484 (surface leakage), there was only minimal evidence of healing using visual assessment techniques.
485 It is suggested that a range of non-destructive techniques such as in-situ permeability testing,
486 ultrasonic techniques and microscopy be employed in future tests to help identify the recovery of
487 mechanical and durability-based properties.

488 The work reported earlier suggested that SS is most effective when healing cracks that are 0.3
489 mm wide or less but in the present case the cracks were wider than this, which may have reduced
490 the healing potential of the system. It is concluded that it would be better to use either a healing
491 agent with a higher viscosity or a different reaction mechanism when a vascular network is required
492 to heal larger cracks (i.e. cracks >0.3 mm in width).

493 The site trials showed that vascular networks can be used at large scale and it has been shown that
494 and the presence of the vascular networks cause the cracks to form in a similar pattern to the vascular
495 network beneath the surface, giving direct access to the healing agent supply. The construction of
496 the vascular networks on site undoubtedly demands additional labour but despite this shortcoming,
497 it is concluded that vascular networks have the potential to heal repeated occurrences of damage.

498 **CONCLUSIONS**

499 A novel technique for creating a vascular network characterised by a series of 2D interconnected

500 hollow channels has been presented. The deployment of this network in both small laboratory and
501 larger structural sized elements has proved successful and has highlighted the potential for its in-situ
502 application to provide a healing mechanism for repeated damage events.

503 A series of preliminary investigations demonstrated the development and refinement of the
504 design of the connectors, whilst the influence of specimen age, flow network location, healing time
505 and curing condition were examined. The preliminary results showed that a small pressure head of
506 0.02 bar was sufficient to ensure that healing agent reached the majority of a crack surface (>90%)
507 within 3 minutes. The greatest coverage of the healing agent on the crack face was achieved when
508 specimens were 14 days old, cured in water, and tested at a CMOD of 0.3 mm.

509 With regards to the healing agents tested it was apparent that although SS was easier to handle
510 and supply into the vascular network, CA offered greater strength recovery (up to 90%) in a
511 significantly shorter time than the SS. This may suggest that CA is the preferred healing agent in
512 applications where rapid healing of damage is required. On the other hand, SS may offer slower
513 healing times and lower levels of healing which may be more suited to low levels of damage in
514 early age structures where there is an abundance of calcium hydroxide in the matrix to facilitate
515 healing. Nevertheless, as with the majority of the tests conducted using autonomic healing agents,
516 there remains considerable uncertainty over the agents suitability for long term encapsulation and
517 its compatibility with the cementitious matrix.

518 Not only do vascular networks provide multiple opportunities to supply a wide range of healing
519 agents but such agents can also be replenished over the lifetime of a structure provided that the
520 channels are emptied at the end of each healing event. With further research, into more efficient
521 methods of forming these networks on site and the identification of compatible healing agents for
522 a range of physical and chemical damage events, vascular networks could provide a viable and
523 efficient healing system in structural elements formed from cementitious materials.

524 **Data Availability Statement**

525 All data created during this research are openly available from the Cardiff University data
526 archive at <http://doi.org/10.17035/d.2020.0107901898>.

Acknowledgments

Financial support from The UK Engineering and Physical Sciences Research Council (EPSRC) for the Resilient Materials for Life (RM4L, EP/02081X/1, 2017-2022) programme grant and Materials for Life (M4L, EP/K026631/1, 2013-2016) grant is gratefully acknowledged. Special recognition is given to Matthieu Goujon, EDF intern student, for his support in carrying out the preliminary experiments and to Martins Pilegis for assistance with the 3D printed materials and site trial work.

REFERENCES

- Belleghem, B. V., Tittelboom, K. V., and Belie, N. D. (2018). "Efficiency of self-healing cementitious materials with encapsulated polyurethane to reduce water ingress through cracks." *Materiales de Construcción*, 68(330), 159 Number: 330.
- Blaiszik, B., Kramer, S., Olugebefola, S., Moore, J., Sottos, N., and White, S. (2010). "Self-Healing Polymers and Composites." *Annual Review of Materials Research*, 40(1), 179–211.
- BS EN 12350-2 (2019). "BS EN 12350-2:2019 - Testing fresh concrete." BSI Standards Limited 2019, Brussels.
- Concrete Society (2010). *Non-structural cracks in concrete: a Concrete Society report*. Concrete Society, London.
- Davies, R. and Jefferson, A. (2017). "Micromechanical modelling of self-healing cementitious materials." *International Journal of Solids and Structures*, 113-114, 180–191.
- Davies, R., Teall, O., Pilegis, M., Kanellopoulos, A., Sharma, T., Jefferson, A., Gardner, D., Al-Tabbaa, A., Paine, K., and Lark, R. (2018). "Large Scale Application of Self-Healing Concrete: Design, Construction, and Testing." *Frontiers in Materials*, 5.
- De Belie, N., Gruyaert, E., Al-Tabbaa, A., Antonaci, P., Baera, C., Bajare, D., Darquennes, A., Davies, R., Ferrara, L., and Jefferson, T. (2018). "A Review of Self-Healing Concrete for Damage Management of Structures." *Advanced Materials Interfaces*, 1800074.
- Dry, C. (1994). "Matrix cracking repair and filling using active and passive modes for smart timed

553 release of chemicals from fibers into cement matrices.” *Smart Materials and Structures*, 3(2),
554 118–123.

555 Dry, C. (2001). “In-service repair of highway bridges and pavements by internal time-release repair
556 chemicals.” *NCHRP-IDEA Program Project Final Report*.

557 Dry, C., Corsaw, M., and Bayer, E. (2003). “A comparison of internal self-repair with resin injection
558 in repair of concrete.” *Journal of Adhesion Science and Technology*, 17(1), 79–89.

559 Dry, C. and McMillan, W. (1996). “Three-part methylmethacrylate adhesive system as an internal
560 delivery system for smart responsive concrete.” *Smart Materials and Structures*, 5(3), 297.

561 Dry, C. M. (1999). “Repair and prevention of damage due to transverse shrinkage cracks in bridge
562 decks.” Vol. 3671, 253–256, <<http://dx.doi.org/10.1117/12.348675>>.

563 Dry, C. M. (2000). “Three designs for the internal release of sealants, adhesives, and waterproofing
564 chemicals into concrete to reduce permeability.” *Cement and Concrete Research*, 30(12), 1969–
565 1977.

566 Formia, A., Terranova, S., Antonaci, P., Pugno, N. M., and Tulliani, J. M. (2015). “Setup of Ex-
567 truded Cementitious Hollow Tubes as Containing/Releasing Devices in Self-Healing Systems.”
568 *Materials*, 8(4), 1897–1923.

569 Gardner, D., Jefferson, A., and Hoffman, A. (2012). “Investigation of capillary flow in discrete
570 cracks in cementitious materials.” *Cement and Concrete Research*, 42(7), 972–981.

571 Gardner, D., Jefferson, A., Hoffman, A., and Lark, R. (2014). “Simulation of the capillary flow of
572 an autonomic healing agent in discrete cracks in cementitious materials.” *Cement and Concrete*
573 *Research*, 58, 35–44.

574 Gardner, D., Lark, R., Jefferson, T., and Davies, R. (2018). “A survey on problems encountered in
575 current concrete construction and the potential benefits of self-healing cementitious materials.”
576 *Case Studies in Construction Materials*, 8, 238–247.

577 Gilabert, F. A., Van Tittelboom, K., Van Stappen, J., Cnudde, V., De Belie, N., and Van Paepegem,
578 W. (2017). “Integral procedure to assess crack filling and mechanical contribution of polymer-
579 based healing agent in encapsulation-based self-healing concrete.” *Cement and Concrete Com-*

580 *posites*, 77, 68–80.

581 Gilford III, J., Hassan, M. M., Rupnow, T., Barbato, M., Okeil, A., and Asadi, S. (2013). “Dicy-
582 clopentadiene and Sodium Silicate Microencapsulation for Self-Healing of Concrete.” *Journal*
583 *of Materials in Civil Engineering*.

584 Hamilton, A. R., Sottos, N. R., and White, S. R. (2011). “Pressurized vascular systems for self-
585 healing materials.” *Journal of The Royal Society Interface*, rsif20110508.

586 Homma, D., Mihashi, H., and Nishiwaki, T. (2009). “Self-Healing Capability of Fibre Reinforced
587 Cementitious Composites.” *Journal of Advanced Concrete Technology*, 7(2), 217–228.

588 Huang, H. and Ye, G. (2011). “Application of sodium silicate solution as self-healing agent in ce-
589 mentitious materials.” *International RILEM Conference on Advances in Construction Materials*
590 *Through Science and Engineering*, Hong Kong.

591 Huang, H., Ye, G., and Shui, Z. (2014). “Feasibility of self-healing in cementitious materials By
592 using capsules or a vascular system?.” *Construction and Building Materials*, 63, 108–118.

593 Joseph, C., Jefferson, A., Isaacs, B., Lark, R., and Gardner, D. (2010). “Experimental investiga-
594 tion of adhesive-based self-healing of cementitious materials.” *Magazine of Concrete Research*,
595 62(11), 831–843.

596 Kanellopoulos, A., Qureshi, T. S., and Al-Tabbaa, A. (2015). “Glass encapsulated minerals for
597 self-healing in cement based composites.” *Construction and Building Materials*, 98, 780–791.

598 Li, V. C., Lim, Y. M., and Chan, Y.-W. (1998). “Feasibility study of a passive smart self-healing
599 cementitious composite.” *Composites Part B: Engineering*, 29(6), 819–827.

600 Li, W., Jiang, Z., and Yang, Z. (2017). “Acoustic characterization of damage and healing of
601 microencapsulation-based self-healing cement matrices.” *Cement and Concrete Composites*, 84,
602 48–61.

603 Maes, M., Van Tittelboom, K., and De Belie, N. (2014). “The efficiency of self-healing cemen-
604 titious materials by means of encapsulated polyurethane in chloride containing environments.”
605 *Construction and Building Materials*, 71, 528–537.

606 Mihashi, H., KANEKO, Y., NISHIWAKI, T., and OTSUKA, K. (2001). “Fundamental study

607 on development of intelligent concrete characterized by self-healing capability for strength.”
608 *Transactions of the Japan Concrete Institute*, 22, 441–450.

609 Mostavi Ehsan, Asadi Somayeh, Hassan Marwa M., and Alansari Mohamed (2015). “Evaluation
610 of Self-Healing Mechanisms in Concrete with Double-Walled Sodium Silicate Microcapsules.”
611 *Journal of Materials in Civil Engineering*, 27(12), 04015035 Publisher: American Society of
612 Civil Engineers.

613 Nishiwaki, T., Mihashi, H., and Okuhara, Y. (2010). “Fundamental Study on Self-Repairing Con-
614 crete Using a Selective Heating Device, <<http://trid.trb.org/view.aspx?id=1203322>> (July).

615 Pareek, S. and Oohira, A. (2011). “A fundamental study on regain of flexural strength of mortars
616 by using a self- repair network system..” Bath, UK, 46–47 (June).

617 Pelletier, M. M., Brown, R., Shukla, A., and Bose, A. (2011). “Self-healing concrete with a
618 microencapsulated healing agent.” *Cement and Concrete Research*.

619 Perez, G., Gaitero, J. J., Erkizia, E., Jimenez, I., and Guerrero, A. (2015). “Characterisation of
620 cement pastes with innovative self-healing system based in epoxy-amine adhesive.” *Cement and
621 Concrete Composites*, 60, 55–64.

622 Sangadji, S. and Schlangen, E. (2012). “Self-healing of Concrete Structures - Novel approach using
623 porous network concrete.” *Journal of Advanced Concrete Technology*, (10), 185–194.

624 Sidiq, A., Gravina, R., and Giustozzi, F. (2019). “Is concrete healing really efficient? A review.”
625 *Construction and Building Materials*, 205, 257–273.

626 Van Tittelboom, K. and De Belie, N. (2013). “Self-Healing in Cementitious MaterialsA Review.”
627 *Materials*, 6(6), 2182–2217.

628 Van Tittelboom, K., De Belie, N., Van Loo, D., and Jacobs, P. (2011). “Self-healing efficiency
629 of cementitious materials containing tubular capsules filled with healing agent.” *Cement and
630 Concrete Composites*, 33(4), 497–505.

631 Van Tittelboom, K., Wang, J., Araújo, M., Snoeck, D., Gruyaert, E., Debbaut, B., Derluyn,
632 H., Cnudde, V., Tsangouri, E., Van Hemelrijck, D., and De Belie, N. (2016). “Comparison of
633 different approaches for self-healing concrete in a large-scale lab test.” *Construction and Building*

634 *Materials*, 107, 125–137.

635 Xue, C., Li, W., Li, J., Tam, V. W. Y., and Ye, G. (2019). “A review study on encapsulation-
636 based self-healing for cementitious materials.” *Structural Concrete*, 20(1), 198–212 _eprint:
637 <https://onlinelibrary.wiley.com/doi/pdf/10.1002/suco.201800177>.

638

List of Tables

639 1 Parametric study on capillary rise and surface coverage of healing agent 27

640 2 Summary of vascular network experimental programme. 28

641 3 Composition of concrete 29

642 4 Strength recovery (H_P) and stiffness recovery (H_K) for twin 1D channel beams (Set 1) 30

TABLE 1. Parametric study on capillary rise and surface coverage of healing agent

Test Series	Specimen Age (days)	Crack width (mm)	No. of channels	Pressure (bar)	Exposure of healing agent(s)	Cover to flow network (mm) [★]
Series 1	14 ^w	0.2	2	0, 0.005, 0.01, 0.02	180	20
Series 2	14 ^w , 140 ^w	0.1, 0.2, 0.3, 0.4	2	0.01	60, 180, 300	20
Series 3	14 [†]	0.2	1	0.01	60, 180, 300	20
Series 4	7 ^w	0.1, 0.2, 0.3, 0.4	1	0.01	180	28, 44

Note. [★] above the underside of the beam, [†] cured in ambient room conditions, ^w cured in water

TABLE 2. Summary of vascular network experimental programme.

	Set 1	Set 2	Set 3	Set 4	Set 5	Set 6
No. of specimens	8	6	6	3	1	2
Specimen dimensions (l x b x d) (mm ³)	255x75 x75	500x100 x100	500x100 x100	600x600 x100	1000x1000 x150	1800x1000 x150
Age at 1 st test (days)	100	7	7	28	28	36
Age at 2 nd test (days)	100	8	35	56	-	231
Healing agent	CA and SS	CA	SS	SS	Water	SS
Notch depth (mm)	5	5	5	None	None	None
Pressure (bar)	0.2	0.2	0.2	0.005	up to 0.5	up to 0.05
Reinforcement (mm)	None	None	None	8	8	10
Curing regime	Ambient	Ambient	Water (20 °C)	Hessian sack	Ambient	Outdoors

TABLE 3. Composition of concrete

Material	Concrete composition (kg/m ³)	
	Sets 1-5	Set 6 Site Trial
Cement	400 (CEM II/B-V 32.5R)	415 (CEMI)
Coarse aggregate (4 - 10 mm crushed limestone)	990	944
Limestone fines (0 - 2 mm)	162	396
Sand (0 - 4 mm marine sand)	648	393
Water	200	179
w/c ratio	0.5	0.43
VS100 (SIKA) plasticiser 1/100 kg cement	0.3	0.35
SIKATARD R retarder 1/100 kg cement	-	0.10

TABLE 4. Strength recovery (H_P) and stiffness recovery (H_K) for twin 1D channel beams (Set 1)

Set 1 test stage (Extracted from typical beam example shown in Fig. 12)	Strength Recovery H_P (%)	Stiffness Recovery H_K (%)
CA Load Cycle 2 Healing	78.6	69.7
SS Load Cycle 2 Healing	17.2	60.5
CA Load Cycle 1 Primary Healing 1	23.4*	1.9*
CA Load Cycle 1 Primary Healing 2	45.1*	14.5*

Note. * uncertainty due to variations in control response.

643

List of Figures

644

645	1	Flow networks setup and connections ready for casting (a) 1D twin network in concrete prism mould (b) Schematic of initial connection design (c) 2D network configuration in concrete prism mould (d) 2D bespoke 3D PLA connection for beam (e) 2D network configuration with 3D PLA connections in concrete prism mould (f) 2D bespoke 3D PLA connection for wall panels	33
646			
647	2	Test setup for three-point bending characterisation of pattern on fracture surface test	34
648			
649	3	Typical fracture surface showing spread of healing agent, a) Series 2: Time 60 s,	
650		(b) Series 2: Time 300 s	35
651			
652	4	Crack coverage as influenced by (a) healing agent pressure; (b) specimen age and healing agent exposure time; (c) specimen curing and healing agent exposure time; and (d) CMOD and cover to network	36
653			
654			
655	5	Flow network from Sets 1-6 (not drawn to scale)	37
656			
657	6	General arrangement of three-point flexural testing	38
658			
659	7	Generic three-point flexural test setup with pressure (a) Supply channels for air and healing agent (b) Pressure supply system	39
660			
661	8	Concrete slab mould flow network set-up (a) specimen 1 (b) specimen 2 (c) general support and loading arrangement	40
662			
663	9	Wall panel testing arrangements (a) Wall panel part assembled prior to casting (b) Schematic of healing agent (HA) injection point (c) Wall panel loading arrangement	41
664			
665	10	Wall panel testing arrangements (a) Wall panel prior to casting (b) Network arrangement and 2D connection detail (c) Vertical cantilever schematic (d) Wall panel prior to testing	42
666			
667	11	Load against CMOD plots for idealised healing in cementitious materials showing the strength and stiffness recovery index terms	43
668			
669	12	Typical repeated healing responses comparing CA, SS and Control in Set 1	44
	13	Load against CMOD for twin channel cyanoacrylate in Set 2	45

670	14	Load and pressure versus CMOD response for twin channel SS and control beams	
671		in Set 3	46
672	15	Load versus CMOD for SS and control beams during re-loading phase in Set 3 . .	47
673	16	Load versus centre displacement of slab for SS vascular network and control slab .	48
674	17	2D channels in slab testing a) 1st stage peak load b) 1st stage after unloading c)	
675		2nd stage loading to failure d) Post-test panel condition for channels at 45° to the	
676		reinforcing bars	49
677	18	Demonstration panel with healing agent supplied (a) Flow network exterior channel	
678		arrangement (b) Filling of flow network and evidence of leakage through crack (c)	
679		Indication of main horizontal crack location and healing agent leakage (d) Post-test	
680		panel condition	50
681	19	Site trial (a) Panel E containing vascular networks with healing agent pump ar-	
682		rangement (b) Closeup of crack with healing agent leaching (c) DIC strain plot	
683		panel E Control with vascular networks at a load of 20 kN	51
684	20	Load versus CMOD for initial and final loading of site trial panel E	52

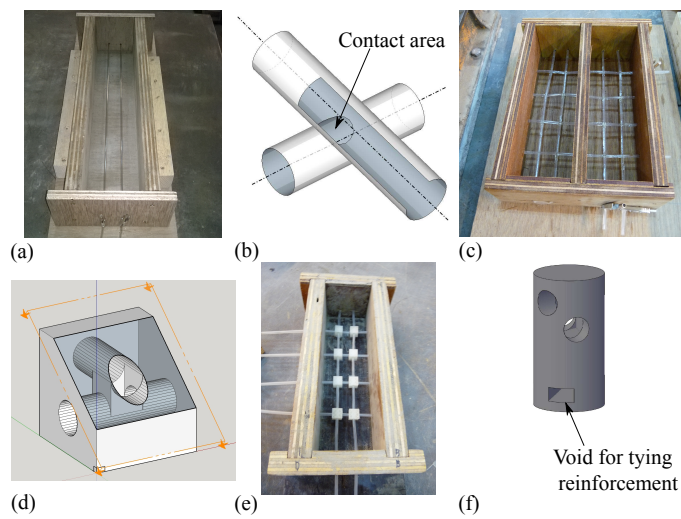


Fig. 1. Flow networks setup and connections ready for casting (a) 1D twin network in concrete prism mould (b) Schematic of initial connection design (c) 2D network configuration in concrete prism mould (d) 2D bespoke 3D PLA connection for beam (e) 2D network configuration with 3D PLA connections in concrete prism mould (f) 2D bespoke 3D PLA connection for wall panels

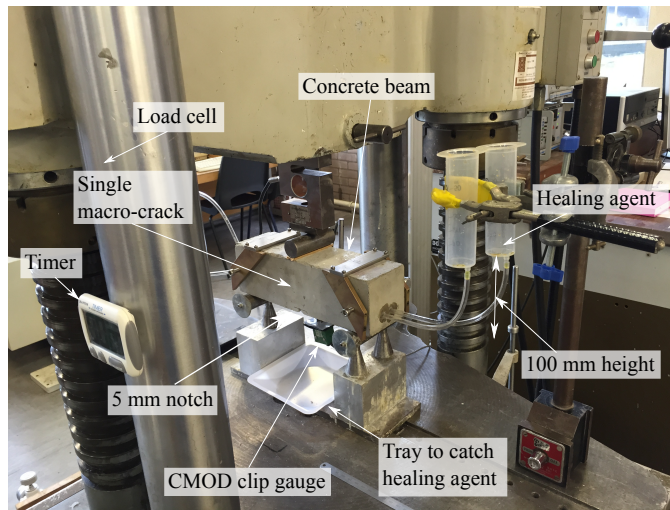


Fig. 2. Test setup for three-point bending characterisation of pattern on fracture surface test

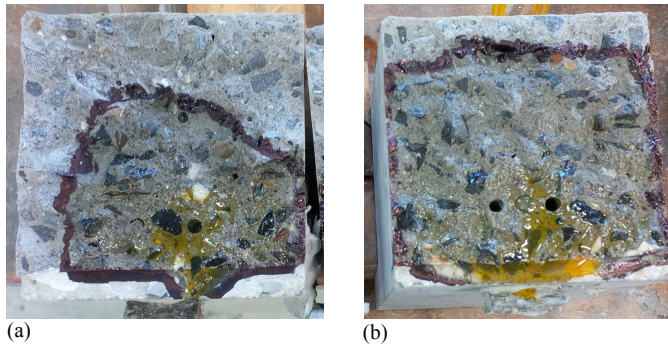


Fig. 3. Typical fracture surface showing spread of healing agent, a) Series 2: Time 60 s, (b) Series 2: Time 300 s

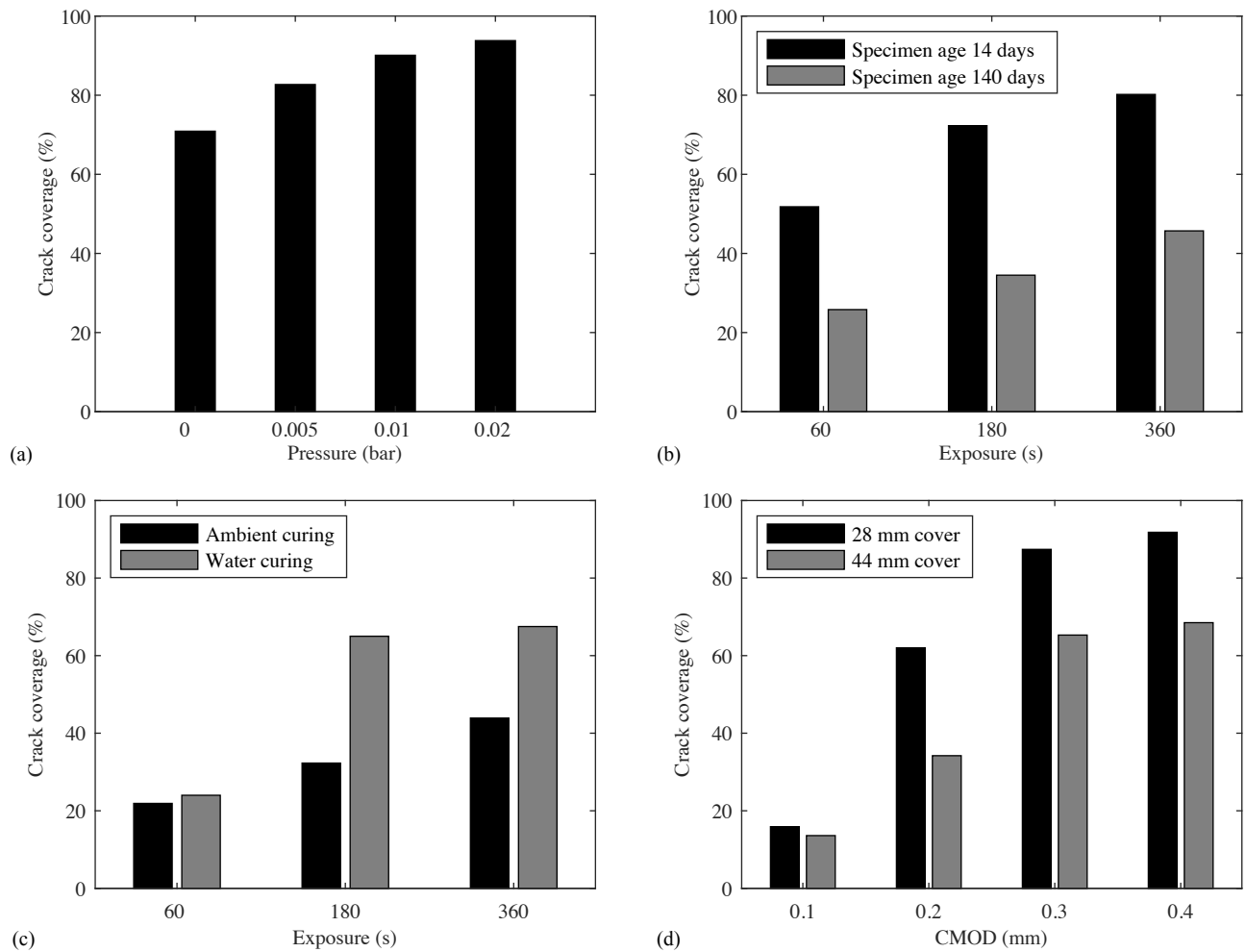


Fig. 4. Crack coverage as influenced by (a) healing agent pressure; (b) specimen age and healing agent exposure time; (c) specimen curing and healing agent exposure time; and (d) CMOD and cover to network

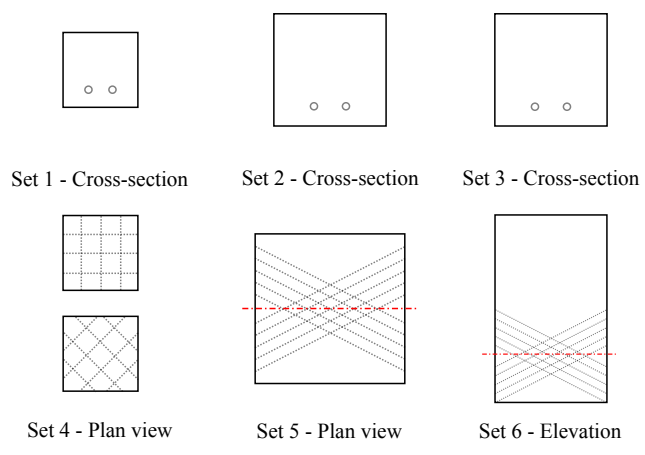


Fig. 5. Flow network from Sets 1-6 (not drawn to scale)

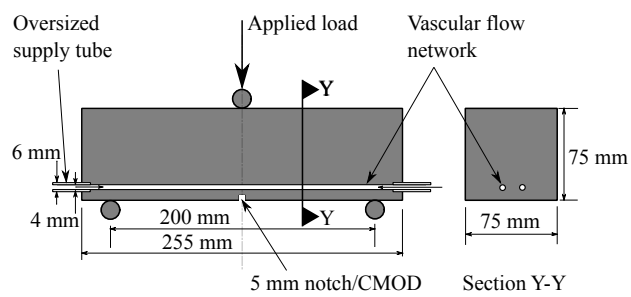


Fig. 6. General arrangement of three-point flexural testing

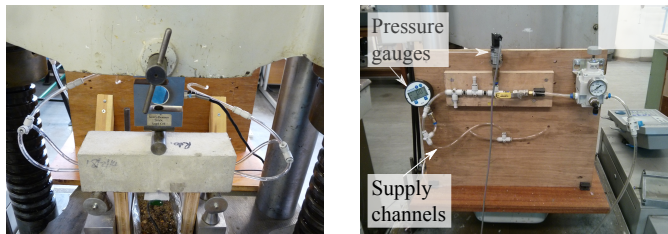
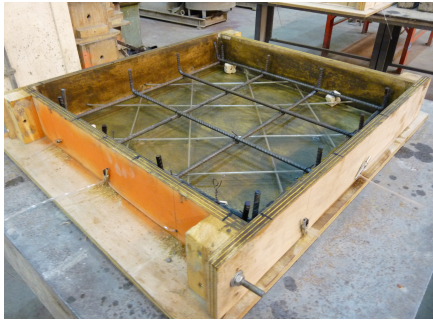


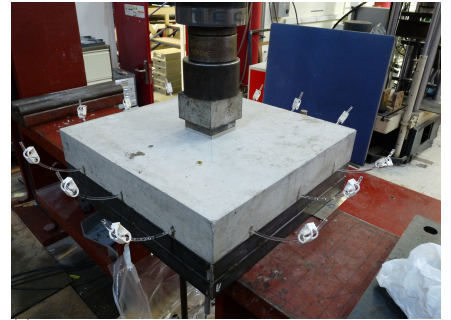
Fig. 7. Generic three-point flexural test setup with pressure (a) Supply channels for air and healing agent (b) Pressure supply system



(a)



(b)



(c)

Fig. 8. Concrete slab mould flow network set-up (a) specimen 1 (b) specimen 2 (c) general support and loading arrangement

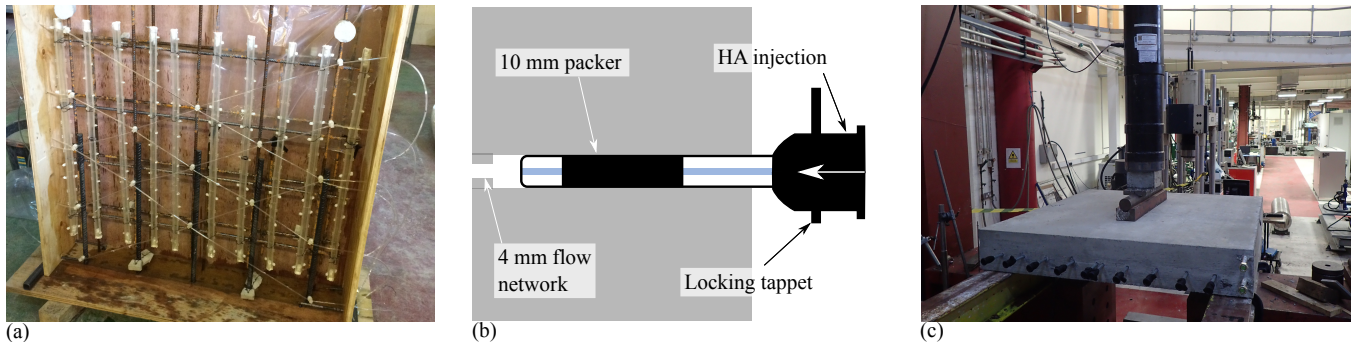


Fig. 9. Wall panel testing arrangements (a) Wall panel part assembled prior to casting (b) Schematic of healing agent (HA) injection point (c) Wall panel loading arrangement

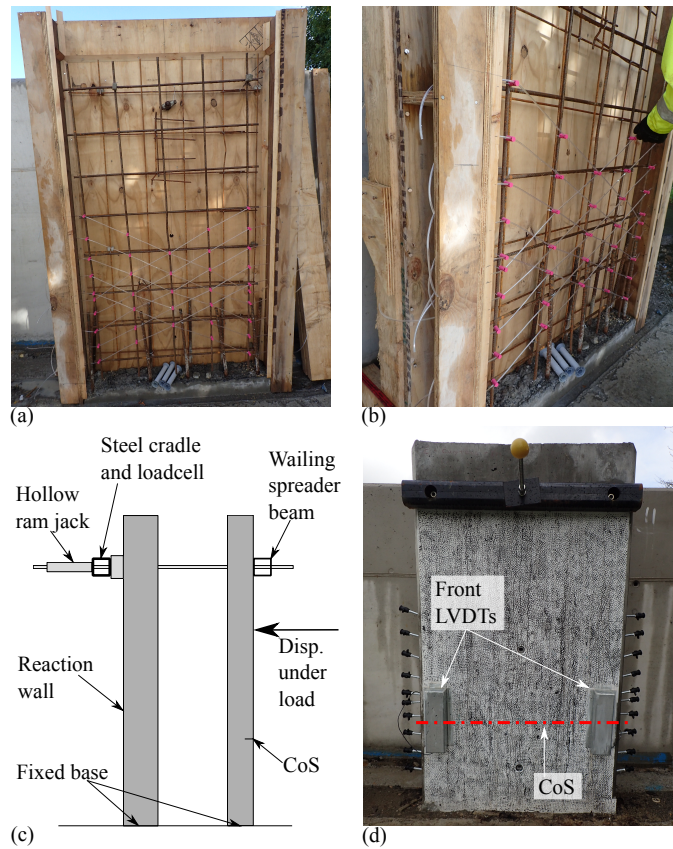


Fig. 10. Wall panel testing arrangements (a) Wall panel prior to casting (b) Network arrangement and 2D connection detail (c) Vertical cantilever schematic (d) Wall panel prior to testing

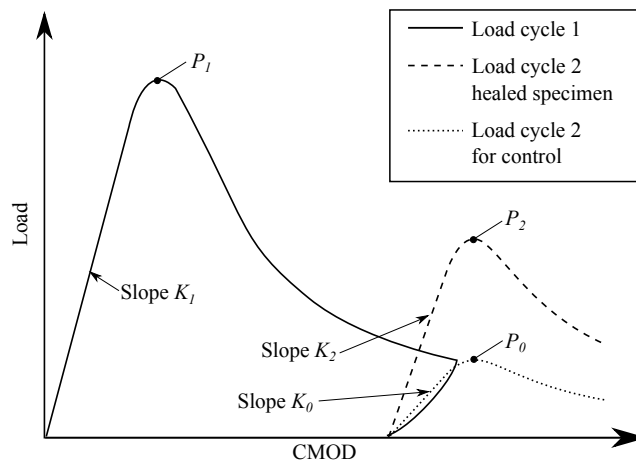


Fig. 11. Load against CMOD plots for idealised healing in cementitious materials showing the strength and stiffness recovery index terms

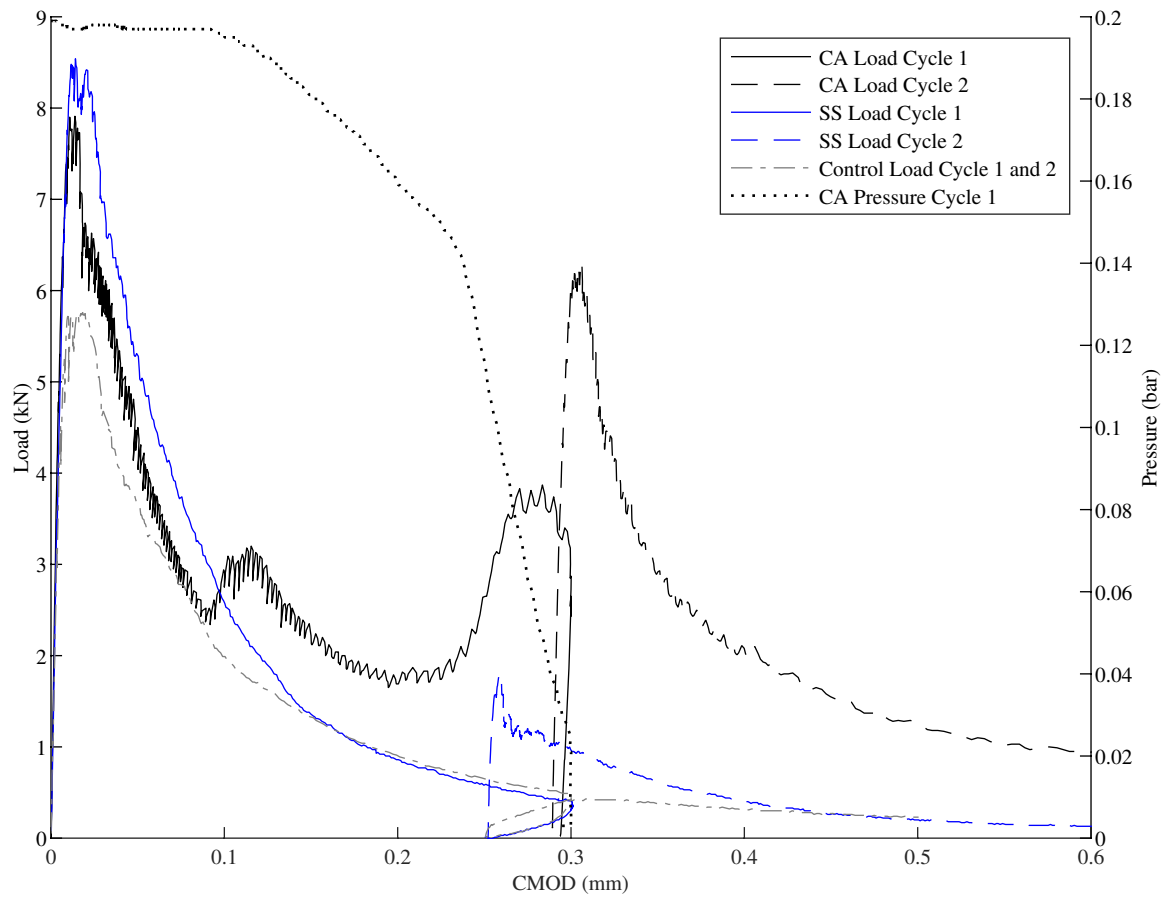


Fig. 12. Typical repeated healing responses comparing CA, SS and Control in Set 1

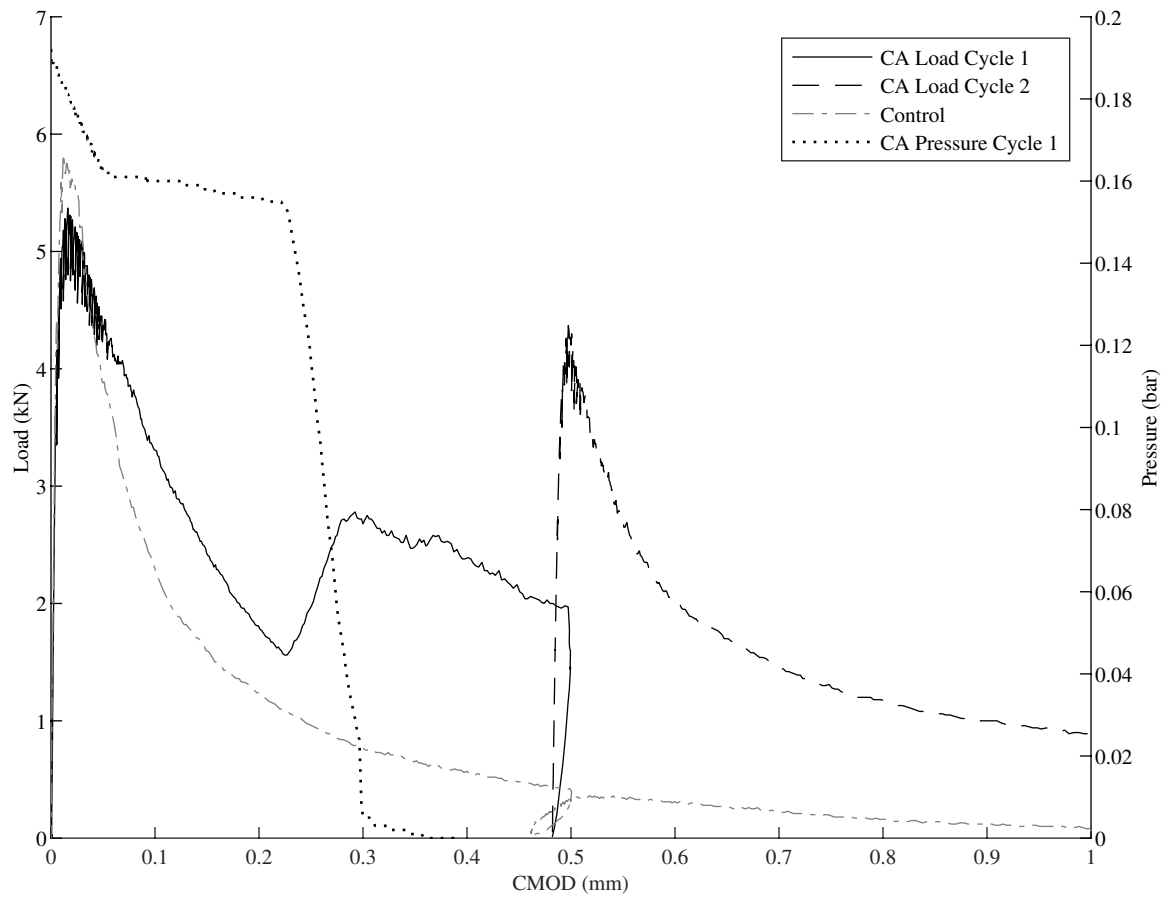


Fig. 13. Load against CMOD for twin channel cyanoacrylate in Set 2

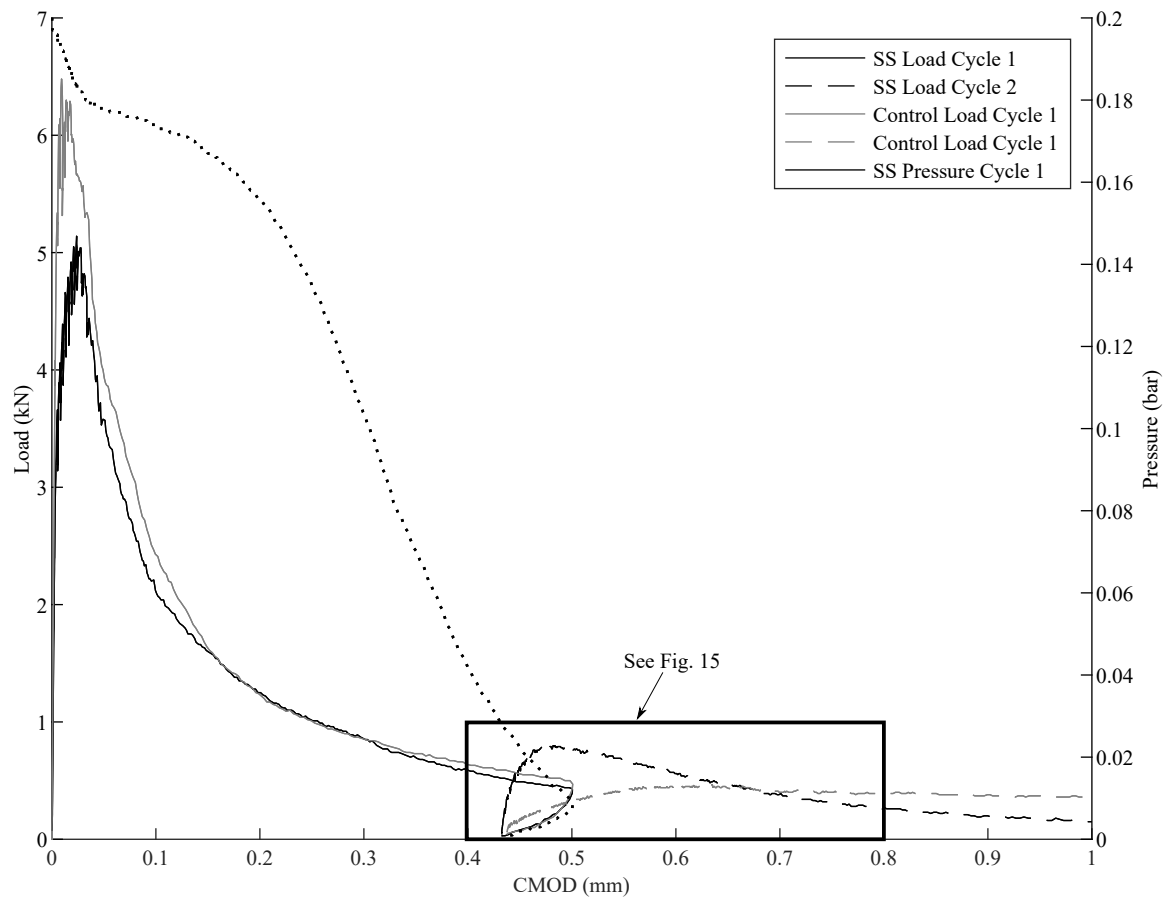


Fig. 14. Load and pressure versus CMOD response for twin channel SS and control beams in Set 3

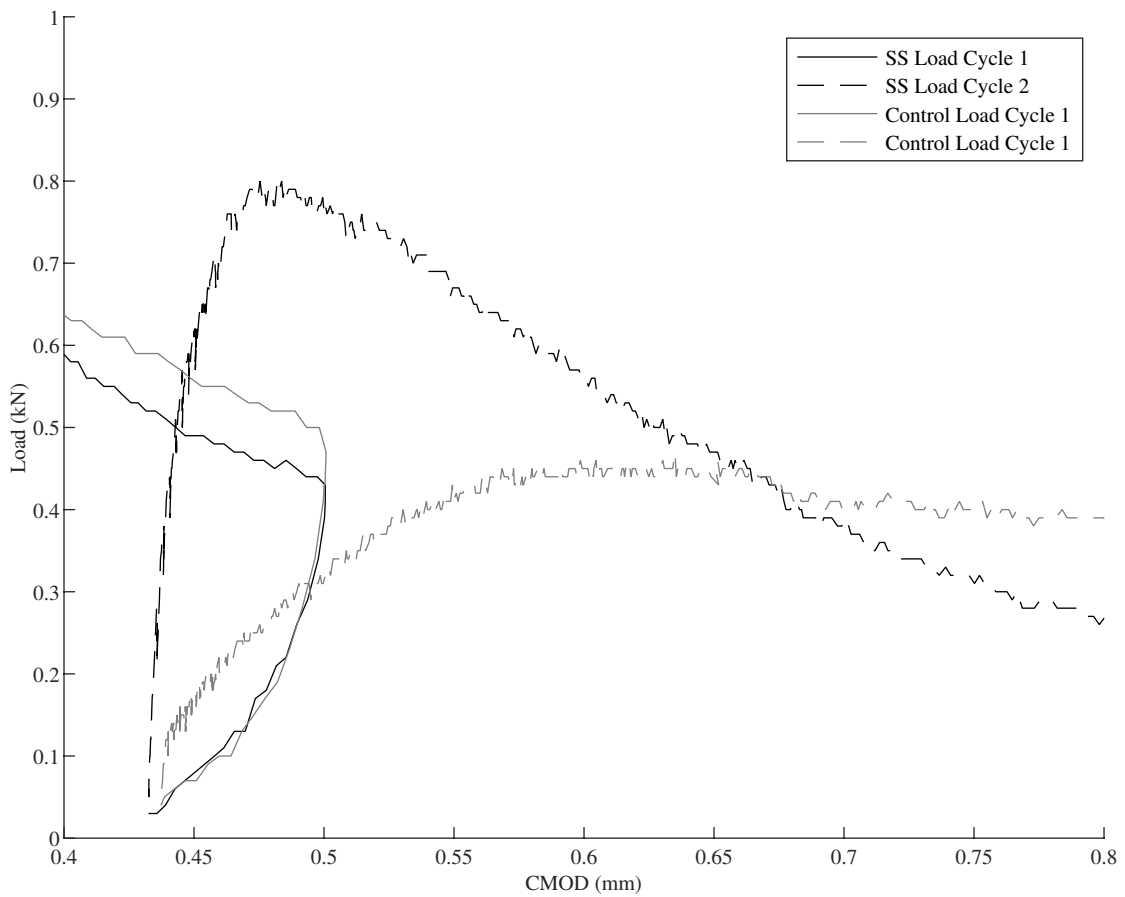


Fig. 15. Load versus CMOD for SS and control beams during re-loading phase in Set 3

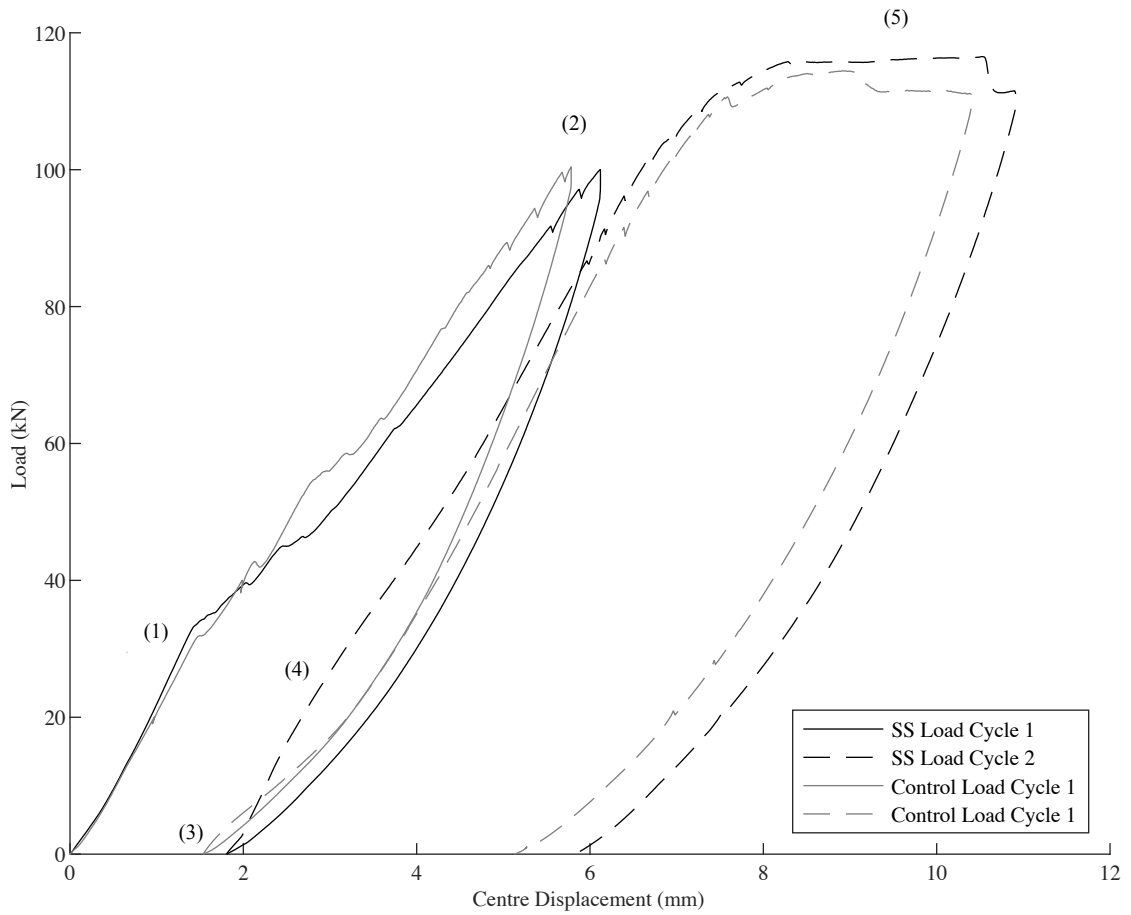


Fig. 16. Load versus centre displacement of slab for SS vascular network and control slab

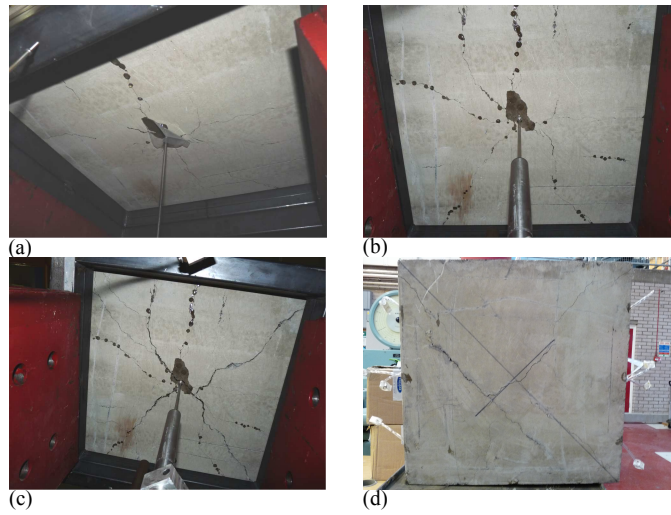


Fig. 17. 2D channels in slab testing a) 1st stage peak load b) 1st stage after unloading c) 2nd stage loading to failure d) Post-test panel condition for channels at 45° to the reinforcing bars

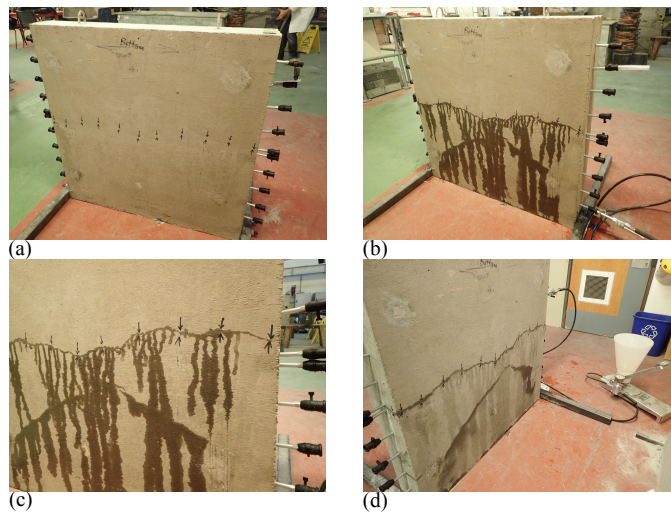


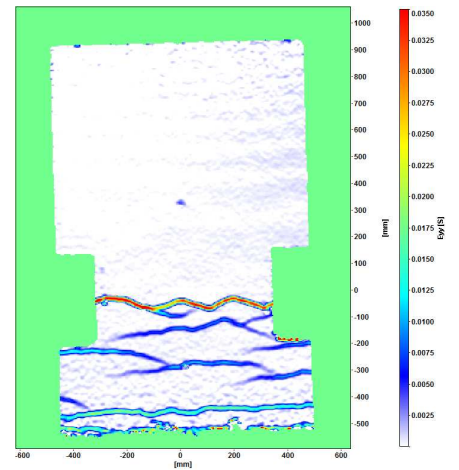
Fig. 18. Demonstration panel with healing agent supplied (a) Flow network exterior channel arrangement (b) Filling of flow network and evidence of leakage through crack (c) Indication of main horizontal crack location and healing agent leakage (d) Post-test panel condition



(a)



(b)



(c)

Fig. 19. Site trial (a) Panel E containing vascular networks with healing agent pump arrangement (b) Closeup of crack with healing agent leaching (c) DIC strain plot panel E Control with vascular networks at a load of 20 kN

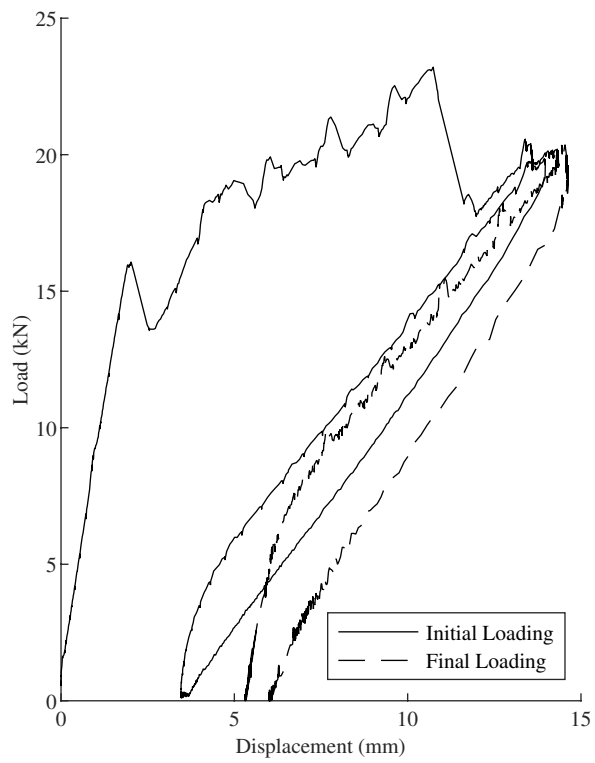


Fig. 20. Load versus CMOD for initial and final loading of site trial panel E